MINERALOGICAL MAGAZINE, JUNE 1978, VOL. 42, PP. 255-63

# A study of iron-bearing rutiles in the paragenesis $TiO_2$-$Al_2O_3$-$P_2O_5$-$SiO_2$

A. PUTNIS

Department of Mineralogy and Petrology, University of Cambridge, Downing Place, Cambridge CB2 3EW

AND

M. M. WILSON

Department of Geology and Mineralogy, University of Queensland, St. Lucia, Queensland 4067

SUMMARY. Hydrothermal rutiles from a suite of rocks at Mount Perry, Queensland, have been studied in thin section, by electron microprobe analysis, and by transmission electron microscopy. The iron-bearing rutiles, while originally single-phase, are found to exsolve a sequence of iron-rich precipitates on experimental annealing, with hematite being formed as the stable equilibrium precipitate. Experiments at different temperatures and annealing times enable a time-temperature-transformation plot to be drawn for the exsolution process. The kinetics of this process are used to conclude that the rutiles formed below about 450 °C.

QUARTZ-RUTILE rich systems, with the association of $Al_2O_3$-$P_2O_5$ phases, although not common, are well documented and the major occurrences described in the literature are in Sweden (Geijer, 1963) and in the U.S.A. (Gross and Parwell, 1968; Ross, 1941). Another deposit with nearly identical assemblages to those previously described occurs in the Mount Perry district, eastern Queensland, located at 25° 12′ N. 151° 40′ E. (fig. 1).

The details of the assemblages, petrography, and petrogenesis of the Mount Perry deposit will be published elsewhere (Wilson, in preparation). This study is mainly concerned with the limits of Fe stability in the rutile and the behaviour of the rutiles during experimental annealing. The experimental results as well as the rutile textures are used to place some limits on the temperature of formation of the rutiles. However, a brief description of the geology is included here for clarity.

The Mount Perry deposit has been briefly examined in the past. Most of the studies have been concerned with the occurrence of rutile and its economic potential and the assessments of the deposit are mainly contained within unpublished company reports. Connah (1957) examined the deposits and described some of the higher-grade rutile areas. Connah considered that the rutile deposits were of hydrothermal origin. Denaro (1976) studied in detail the area described by Connah, particularly the nature of the rutile deposits and the brecciation associated with higher concentrations of rutile. Aspects of the assemblages in the surrounding rocks were also studied.

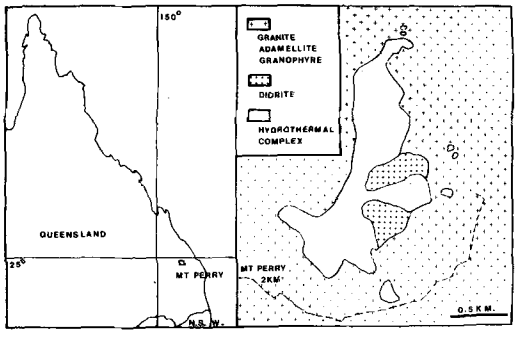


MT PERRY HYDROTHERMAL COMPLEX
GENERAL GEOLOGY

FIG. 1

*Geology.* The quartz-rutile deposit is located within the Mount Perry complex, a system of calc-alkaline, magmatic rocks of predominantly intrusive origin. It forms part of a continuous belt of similar rocks stretching from Biggenden in the south, 25° 4′ N. 152° 4′ E. to Gladstone in the north, 24° 9′ N. 151° 8′ E. Within the belt several calc-alkaline complexes occur as well as porphyry copper systems.

The quartz–rutile mass lies immediately to the east of the Mount Perry township and forms the spine of the Boolbunda Range. It is underlain by adamellites, tonalites, granites, and granophyres and is intruded by minor microdiorites and rhyolitic dykes. The eroded remnant is approximately 300 m thick at the southern end, forming Mount Perry proper and thins northwards over a distance of approximately 2–3 km. Another similar mass occurs approximately 2 km further north of the main deposit. The geology of the area is shown in fig. 1.

Within the hydrothermal complex the rocks are subdivided into three major, vertically disposed zones. The basal zone is an aluminosilicate–phosphate zone, followed by a mica-rich zone usually devoid of other aluminosilicates, and finally, the upper quartz-rich zone.

The basal zone is the most mineralogically complex and corundum, diaspore, andalusite, pyrophyllite, kaolinite, muscovite, sericite, alums (K and Na), jarosite (K and Na), phosphates (Mg, Fe, Al, Na–Ca, Sr), rutile, pyrite, hematite, and magnetite occur, often with many of them in the one rock, or more commonly as groups. Thus corundum, diaspore, kaolinite, and pyrophyllite may occur in association; the phosphates tend to occur together and mica and rutile may occur in all rocks.

Following the basal aluminosilicate–phosphate zone is the mica-rich zone. In some parts of the section the rock consists wholly of mica–rutile–pyrite, devoid even of quartz. More commonly the rock consists of major amounts of mica and rutile with varying proportions of quartz and pyrite. The thickness and continuity of the zone is variable, thickest at the southern end, thinning rapidly to the central area, and thickening again towards the north, directly above a thicker aluminosilicate zone.

The upper quartz-rich zone is volumetrically the most important. Usually the rock contains only quartz and rutile, or with varying amounts of pyrite. Proportions vary with quartz 95–9%, rutile 1–5%, pyrite 1–5%, mica less than 1%.

Geijer (1963) described the deposits from Hållsjöberget, Dicksberget, and Västanå in Sweden as areas where significant deposits contain complex associations of Al-P-Ti-Si bearing minerals. A wide variety of mineral types is present in the assemblages, but quartz-rutile-aluminosilicates and Fe-Mg-Al phosphates predominate. Similarly, Ross (1941) and Gross and Parwell (1968) have described deposits at Graves Mountain and White Mountain with close similarities to the Swedish occurrences. There is a close parallel between the different deposits. Although some variation in the occurrence of particular phases is noted, the assemblages fall broadly into the following groups: quartz, oxides of Fe–Ti, sulphides, aluminates, aluminosilicates, phosphates, sulphates. Hydrothermal-metasomatic processes are considered to be responsible for all of these deposits. (Geijer, 1963; Esphenshade and Potter, 1960; Wilson, in preparation).

The *rutile textures* are considered to be important indicators of the time sequence of hydrothermal-metasomatic events and thus bear directly on the interpretation of Fe substitution in the rutiles and their temperature of formation. Broadly, rutile occurs in four principal settings: as inclusions in quartz, always as fine euhedral prisms or very fine stellate clusters of prisms; at triple junctions between polygonal quartz grains (multiple junctions in three dimensions); as massive veins in brecciated zones, usually as very fine-grained rutile; as replacements of pre-existing Fe–Ti oxides, retaining the textural habit of those oxides.

Polygonal rutile grains are the most common mode of occurrence of the coarser rutile grains and they show a consistent relationship to the surrounding matrix of quartz. Quartz, which forms the bulk of the rock volume is markedly polygonal, closely resembling the 'foam' or 'soap bubble' structure (Chadwick, 1972). Rutile also develops a similar form to the surrounding quartz grains, and thus occurs at triple junctions in thin sections (fig. 2). Microscopic examination of the separated rutile grains shows that they are equant polygons

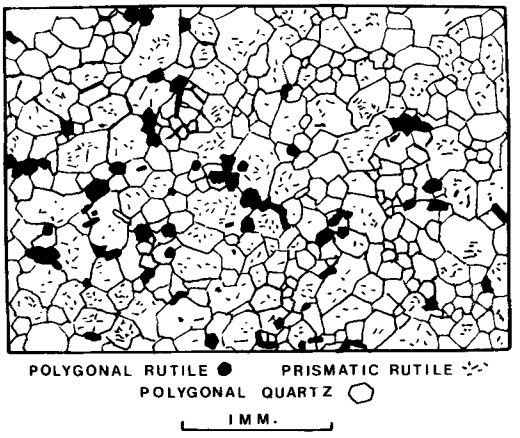


FIG. 2. Polygonal rutile set at triple junctions between polygonal quartz grains. Finer euhedral, prismatic rutile is included in the quartz. Drawn from a photomicrograph.

without a tendency to terminate or develop crystal faces or to develop the characteristic prismatic form.

The rutile grains are not interstitial in the sense of a major-phase–minor-phase intergrowth where the minor phase simply fills the residual space between the major-phase grains. The interpretation accorded to the polygonal nature of the intergrowths is that they have formed simultaneously with quartz, and that their form is the result of mutual interaction during growth. Since both phases are polygonal in form, and junctions between grains are close to 120°, it probably indicates that their surface energies are sufficiently close to each other to prevent markedly dimensional habits from developing in either phase.

The texture is not due to a post-deformation recrystallization annealing event. The underlying granitic rocks are undeformed and there is some textural evidence in the rocks to suggest a static replacement process.

Fine-grained rutile is included in quartz grains, often in significant volumes and commonly adopts a habit of very fine-grained, stellate clusters of prisms which may cross quartz–quartz boundaries without disruption. This form is seen in rocks, usually in the upper, quartz-rich section of the system, where quartz is very fine-grained with interlocking sinuous boundaries similar to those seen in fine-grained cherts. In the areas where the quartz is polygonal the included rutile is somewhat coarser-grained than the stellate prism form and occurs as isolated doubly terminated prisms. These grains may also show some crossing of quartz–quartz boundaries, especially where they form in an area marginal to the massive veins. These rutile grains are suggested to have nucleated partly prior to and partly contemporaneously with quartz.

Rutile veining takes the form of both distinct infilling after brecciation with typically sharp junctions with the surrounding rock or as gradational vein infillings where there is an apparently steady increase in rutile concentration from the normal quartz-rich rock to a pure rutile vein. Macroscopically this is seen as a colour gradation from the nearly pure white of the surrounding granular quartz–rutile to the brown, massive rutile vein. These gradational veins show a banding parallel to the elongation of the vein, although there is no obvious microstructure seen in thin section such as grain elongation. The texture resembles a fluxion banding, although it is not thought to have been produced by flow in a molten liquid. Colour and grain size appear to be the main cause of the banded character. No growth orientation of the rutile normal to the vein wall is observed, i.e. no cockade growth in open spaces.

In general the brecciated area of the deposit has the appearance of disruption due to forcible injection and the rutile veining, in part, appears to be pneumatolytic. The gradational veins may be due to a form of segregation banding although the evidence is not conclusive.

Other rutile is clearly the result of replacement of pre-existing Fe–Ti oxides. Rutile in this habit tends to be subordinate in terms of areal abundance and is found mainly in the upper zone of the system. Fine-grained quartz with a cherty appearance is also characteristically associated with rutile with pseudomorphic forms.

Replacement of Fe–Ti oxides in volcanic and other rocks is usually an oxidative process, but it may also be the result of replacement involving sulphur, whereby ilmenite is transformed to rutile plus pyrite. This is considered to have been the main process at Mount Perry and have produced the above-mentioned pseudomorphic textures. All other components, except silica, have been removed in the replacement process. The thermodynamic stability of ilmenite under varying conditions of $f_S$ and $f_{O_2}$ are considered elsewhere (Wilson, in preparation).

Pseudomorphic textures, where the form of magnetite or ilmenite is retained, are characteristic of replacement of Fe–Ti oxides (Haggerty, 1976) and may be produced by purely oxidative processes. Haggerty lists replacements of ilmenite where products may include intermediate ferrian rutile. In the Mount Perry deposit, Fe contents of rutiles are generally low (Table I). Pseudobrookite may also be produced, as at Graves Mountain, but has not been identified in this deposit.

Rutile deposition is considered to have spanned the spectrum of thermal and compositional ranges of the alteration process that produced the Mount Perry deposit. Pre-existing rocks, some certainly of volcanic origin, have been subjected to an intense hydrothermal alteration process, which has produced a silica-rich rock with subordinate amounts of the other components. The alteration process produced rutile in the earlier stages through alteration of Fe–Ti oxides in the system. Other rutile was produced in the earliest stages of alteration directly from the hydrothermal solution and continued forming throughout the whole period of hydrothermal activity, which terminated as a pneumatolytic event producing rutile veining. The rutile deposition is, therefore, seen as preceding, contemporaneous with, and following the deposition of quartz.

*Chemistry of the rutiles.* Although rutile is essentially $TiO_2$, smaller amounts of a range of elements are detected in chemical analyses. Analyses of rutile (Deer *et al.*, 1966) show varying amounts of FeO,

$Fe_2O_3$, $Cr_2O_3$, $Al_2O_3$, $Nb_2O_5$, $Ta_2O_5$, MnO, $SnO_2$, and $SiO_2$. El Goresy and Ramdohr (1975) list the compositions of rutiles containing $ZrO_2$, MgO, and CaO in addition to the above-mentioned elements. The substitution of $Fe^{2+}$ and $Fe^{3+}$ may be electrostatically balanced by either the substitution of an ion of higher valence state than $Ti^{4+}$, such as $Nb^{5+}$ or $Ta^{5+}$, or balanced by lattice vacancies (Deer *et al.*, 1966). Balanced charge structures would imply a $(2R^{5+}+R^{2+})$ substitution for $3Ti^{4+}$, or $(R^{5+}+R^{3+})$ for $2Ti^{4+}$, or the replacement of $2Ti^{4+}$ by $(2R^{3+}+R^{2+})$.

Low-pressure phase equilibria (Lindsley, 1976) indicate that only limited $Fe_2O_3$ solid solution will occur in rutile. This may be as high as *c.* 5 mole% $Fe_2O_3$ at 1650 °C, but at geologically reasonable temperatures, particularly in the range indicated for the Mount Perry system, less than 1 mole% substitution is indicated. The solubility of Fe alone in rutile has been determined by Wittke (1967) at 1 atom oxygen pressure in the range 800 to 1350 °C, where it increases from 1 atom% to 3 atom%. Lindsley cites $Fe_2O_3$ as the most common impurity in rutile.

Analyses of rutiles from Mount Perry are listed in Table I. The analyses were carried out with an energy-dispersive electron microprobe comprising a Si(Li) solid-state detector and Harwell pulse processor (Kandiah *et al.*, 1975) interfaced to a Data General Nova 1220 minicomputer with 20 K core storage. The results were calculated using a computer program employing the iterative spectrum stripping technique (Statham, 1976).

The results of the analyses show that the major substitutions are $SiO_2$, $V_2O_5$, and $FeO$–$Fe_2O_3$. $SiO_2$ may be absent or as high as 1·28%. This higher than average value may be the result of fluorescence from surrounding quartz grains as the

TABLE I. *Mount Perry rutile analyses*

| | P1 | P6 | P7 | P9 | P10 | P11 | P12 | P14 | P18 | P19 | P23 | P28 |
|---|---|---|---|---|---|---|---|---|---|---|---|---|
| $TiO_2$ | 97·599 | 98·27 | 97·45 | 98·376 | 98·344 | 98·48 | 98·119 | 97·639 | 97·13 | 97·533 | 97·879 | 97·42 |
| $SiO_2$ | 0·569 | 1·13 | 0·88 | 0·219 | 0·567 | 0·59 | 0·706 | 0·209 | 1·15 | 0·680 | 0·534 | 0·41 |
| $V_2O_5$ | 0·444 | 0·47 | 0·47 | 0·416 | 0·791 | 0·81 | 0·460 | 0·781 | 0·91 | 0·654 | 0·601 | 1·25 |
| FeO | 0·846 | 0·62 | 0·82 | 0·847 | 0·362 | — | 0·317 | — | 0·58 | 0·773 | 0·726 | 0·29 |
| $Al_2O_3$ | — | — | — | — | — | — | — | — | — | — | — | — |
| $Cr_2O_3$ | — | — | — | — | — | — | — | 0·311 | — | — | — | — |
| CaO | — | — | — | 0·140 | — | — | — | 0·090 | — | — | — | — |
| Total | 99·458 | 100·49 | 99·62 | 99·998 | 100·064 | 99·88 | 99·602 | 99·03 | 99·67 | 99·64 | 99·74 | 99·37 |
| | | | | | *Ions on the basis of 2 oxygens* | | | | | | | |
| Ti | 0·9827 | 0·9773 | 0·9789 | 0·9868 | 0·9817 | 0·9832 | 0·9837 | 0·9889 | 0·9756 | 0·9895 | 0·9848 | 0·9808 |
| Si | 0·0076 | 0·0149 | 0·0011 | 0·0029 | 0·0075 | 0·0078 | 0·0094 | 0·0027 | 0·0139 | 0·0007 | 0·0071 | 0·0042 |
| V | 0·0019 | 0·0041 | 0·0062 | 0·0018 | 0·0035 | 0·0035 | 0·0020 | 0·0034 | 0·0120 | 0·0029 | 0·0026 | 0·0165 |
| $Fe^{2+}$ | 0·0094 | 0·0062 | 0·0123 | 0·0094 | 0·0040 | — | 0·0035 | — | 0·0087 | 0·0078 | 0·0081 | 0·0043 |
| $Fe^{3+}$ | 0·0042 | 0·0028 | 0·0055 | 0·0042 | 0·0018 | — | 0·0015 | — | 0·0040 | 0·0039 | 0·0037 | 0·0019 |
| Al | — | — | — | — | — | — | — | — | — | — | — | — |
| Cr | — | — | — | — | — | — | — | 0·0016 | — | — | — | — |
| Ca | — | — | — | 0·0020 | — | — | — | 0·0012 | — | — | — | — |

| | P30 | P32 | P33 | P38 | P40 | P44 | P53 | P55 | P61 | P62 | P66 |
|---|---|---|---|---|---|---|---|---|---|---|---|
| $TiO_2$ | 98·17 | 98·66 | 98·337 | 98·187 | 98·649 | 98·41 | 98·97 | 98·198 | 98·330 | 98·43 | 98·675 |
| $SiO_2$ | 0·43 | — | 0·266 | 0·352 | 0·603 | 0·88 | — | 1·282 | 0·664 | 0·160 | 0·193 |
| $V_2O_5$ | 0·381 | 0·28 | 0·305 | 0·588 | 0·471 | 0·31 | 0·76 | 1·025 | 0·720 | 0·530 | 0·876 |
| FeO | 0·390 | 0·550 | 0·459 | 0·167 | 0·266 | — | 0·27 | 0·409 | 0·141 | 0·862 | 0·489 |
| $Al_2O_3$ | 0·46 | — | — | — | — | — | — | — | — | — | — |
| $Cr_2O_3$ | 0·153 | — | 0·463 | — | 0·268 | — | — | — | — | — | — |
| CaO | — | — | — | — | — | — | — | — | — | — | — |
| Total | 99·984 | 99·49 | 99·83 | 99·294 | 100·257 | 99·60 | 100·00 | 100·91 | 99·855 | 99·98 | 100·233 |
| | | | | | *Ions on the basis of 2 oxygens* | | | | | | |
| Ti | 0·9831 | 0·9939 | 0·9868 | 0·9879 | 0·9800 | 0·9833 | 0·9929 | 0·9695 | 0·9824 | 0·9895 | 0·9820 |
| Si | 0·0057 | — | 0·0035 | 0·0046 | 0·0079 | 0·0132 | — | 0·0170 | 0·0088 | 0·0021 | 0·0034 |
| V | 0·0016 | 0·0025 | 0·0013 | 0·0025 | 0·0020 | 0·0014 | 0·0067 | 0·0044 | 0·0031 | 0·0023 | 0·0038 |
| $Fe^{2+}$ | 0·0039 | 0·0055 | 0·0051 | 0·0018 | 0·0029 | — | 0·0027 | 0·0045 | 0·0016 | 0·0096 | 0·0054 |
| $Fe^{3+}$ | 0·0019 | 0·0025 | 0·0023 | 0·0008 | 0·0013 | — | 0·0012 | 0·0026 | 0·0007 | 0·0043 | 0·0024 |
| Al | 0·0036 | — | — | — | — | — | — | — | — | — | — |
| Cr | 0·0080 | — | 0·0024 | — | 0·0014 | — | — | — | — | — | — |
| Ca | — | — | — | — | — | — | — | — | — | — | — |

rutile in sample P55 is very fine grained. Other samples were separated from the rocks and mounted in resins for microprobe analysis and the $SiO_2$ levels in these analyses are between 0·2 and 0·5%. $SiO_2$ for $TiO_2$ is an apparently straightforward charge balanced substitution limited principally by the size of the ions.

The main feature of the analyses is the vanadium and iron contents. The combination of the two oxides usually accounts for 1·2 to 1·3% of the total, with either being the main proportion. In some grains no iron was detected (P11, P14, P44). Vanadium was present in all specimens. Minor amounts of CaO and $Al_2O_3$ were also detected in some samples. As the rutiles in the Mount Perry rocks have a polygenetic origin, the rutile analyses reflect various changes in the chemistry of the system. Some of the elements in the rutiles were derived *in situ* whereas others came directly from hydrothermal solution.

Pre-existing Fe–Ti oxides would contain vanadium (especially Mt–$Usp_{ss}$). During an alteration process where rutile was produced, the vanadium could have been derived directly from the Fe–Ti oxide. Sample P9 is a rutile with a texture that indicates replacement of either magnetite or ilmenite. P23 is a rutile from a granitic rock where the rutile is apparently of magmatic origin, although some alteration can be detected in the surrounding rock. Other rutiles are considered to be wholly of hydrothermal origin.

Thus vanadium and iron are thought to have been derived from a variety of sources depending upon the way in which the rutile formed; partly from *in situ* sources and partly from hydrothermal sources as noted above.

*Electron microscope observations of the rutiles.* A number of the separated rutiles were prepared for electron microscopy by crushing the grains under alcohol in an agate mortar. The finest particles were collected from suspension and mounted on a standard carbon-coated grid for observations in an AEI EM6G transmission electron microscope operated at 100 kV. The original aim of the electron microscopy was to determine whether the minor element contents were due to fine scale intergrowths or inclusions, or whether they were part of a solid solution in the rutile. The following rutiles were examined: P6, P11, P18, P23, P32, P44, P62, P66.

Apart from P23 which will be discussed separately, none of the samples showed any significant microstructural intergrowths, and it was therefore assumed that the minor element impurities were present in solid solution. The rutiles were generally homogeneous and devoid of any noteworthy features, apart from (011) twin planes, which occurred with variable density throughout the samples, and polyhedral cavities, which were assumed to be liquid or gaseous inclusions.

Sample P23 contained infrequent blade-like lamellae of a precipitate phase, occurring in two sets on rutile (100) planes. The lamellae were coherent with the matrix, and their presence produced no change in the electron diffraction pattern of the rutile. The lamellae were approximately 1000–2000 Å long and 100 Å wide.

Thicker grains can be annealed *in situ* in the electron microscope, either by direct beam heating or by heating an adjacent grain causing heat to be transferred to the grain under observation. The latter method ensures that the electron radiation plays no direct role in the annealing experiment. Although the temperature cannot be measured in such *in situ* experiments, it can be controlled by focusing, defocusing, and lateral shifts of the beam.

When the rutile samples were beam-heated in this way all of the iron-bearing rutiles spontaneously exsolved very fine platelet-like precipitates. These platelets occurred in two sets, parallel to the (100) planes of the tetragonal rutile structure.

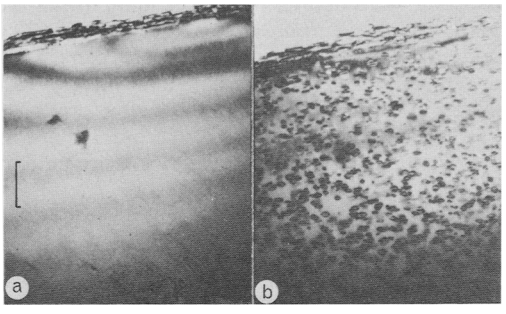


FIG. 3. (*a*), a typical, homogeneous rutile grain before experimental annealing. (*b*), the same grain after beam annealing, showing the formation of small precipitates. Observations in a number of orientations indicates that the precipitates are small platelets on (100) planes of the rutile. The length of the scale bar is 0·2 μm.

Fig. 3 shows a typical grain before and after beam annealing. The formation of these platelets has no noticeable effect on the electron-diffraction pattern of the rutile, and observations of the contrast mechanisms indicate that the precipitates are strained, coherent, and disc-shaped. The fact that no such behaviour was observed in P11 and P44, which contain no measurable iron, suggests that the exsolution is due to the presence of iron, and hence that the platelets are iron-rich. Further evidence for this will be given below. The morphology, homogeneous distribution, coherency, and solute-rich composition of the platelets, as well as

the fact that they have a structure similar to that of the rutile matrix suggests that they are analogous to Guinier–Preston (G.P.) zones. G.P. zones are the first-formed coherent precipitates in a system where the matrix and the equilibrium exsolution product differ significantly in structure, so that direct nucleation of this equilibrium phase is kinetically difficult. G.P. zones have been described in a large number of metal systems (Chadwick, 1972) and in some minerals (Champness and Lorimer, 1976).

*Experimental annealing of the rutile.* Longer-term annealing experiments were carried out to determine the nature of the stable equilibrium precipitate. The separated rutile grains were placed in gold tubes (inside diameter 1 mm), which, after evacuation, were sealed by welding with a DC carbon arc. The tubes were collapsed under a hydrostatic pressure of 1000 atm and annealing experiments carried out, in the absence of vapour, in a calibrated dry furnace.

The results of these experiments show that the stable equilibrium precipitate is a phase whose diffraction pattern can be indexed on the hematite structure, and whose lattice parameters indicate a composition hematite, 0–20% ilmenite, using the relationship determined by Lindsley (1965). Isothermal annealing experiments were carried out at temperatures between 400 and 650 °C for different times, and the charges, after crushing, were examined in the electron microscope. In this way the exsolution process could be followed as a function of temperature and time.

The results show that hematite forms only after the formation of two transitional phases. First, in short-term annealing runs, the fully coherent platelets, similar to those observed in the *in situ* experiments form. Secondly, an intermediate phase with similarities to both the rutile structure and the hematite structure forms, and finally after longer annealing times the stable hematite phase forms. Such a precipitation sequence illustrates the general principle that if the direct formation of the stable phase is kinetically impeded, transitional phases, more similar in structure to the matrix, will form. The similarity in structure reduces the interfacial free energies between the precipitate and matrix, thereby reducing the activation energy for nucleation. The mechanism of this exsolution process and the crystallographic relations between the phases is discussed elsewhere (Putnis, 1977). In this paper we are primarily interested in the kinetics of the process and the applications to the paragenesis of the rutiles.

The volumes of the three phases formed relative to the concentration of iron in the matrix indicate that the iron content of the precipitates also increases in a stepwise manner. The coherent phase formed in the *in situ* experiments is probably enriched in iron by a factor of about 10 relative to the matrix. The intermediate phase has a composition of the form $(Fe, Ti)_2O_3$ with the possibility of variable amounts of iron (Putnis, 1977). The composition of the hematite phase results in a very small volume of this precipitate present in the runs.

*Time–temperature–transformation diagram.* The annealing experiments allow a time–temperature–transformation (*TTT*) plot to be constructed for the exsolution process. The experiments were carried out on sample P32 and the results are shown in fig. 4. Most of the experimental runs were carried out to determine the onset of precipitation of the G.P. zones and no attempt was made to estimate the fraction of the reaction completed. The solid curve of fig. 4 thus indicates the

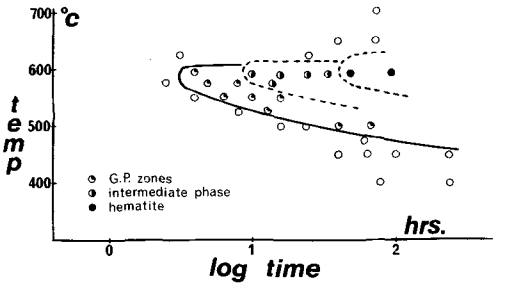


FIG. 4. An experimental *TTT* curve illustrating the kinetics of the formation of G.P. zones, the intermediate phase, and hematite from the rutile solid solution. All of the lines drawn mark the beginning of precipitation of the phases.

start of coherent precipitation. Similar curves can be constructed for the intermediate phase and for hematite, although a degree of uncertainty is introduced in the latter case due to the difficulty in locating the relatively small volume of precipitate in the crushed grains. The curves for these phases are drawn in dotted lines in fig. 4, as they are based on few data points, and on the assumption that their slopes are parallel to the curve for the coherent precipitate. This assumption is justified if the diffusion mechanism is the same in each case, and considering the similarity in the temperatures of formation of the phases, it would be reasonable to assume that this was so.

There are a number of features of the *TTT* diagram relevant to the present study. First, runs at 625 °C and above produced no precipitates even at long annealing times, whereas at 592 °C the hematite phase was present in the runs after similar times. This suggests that the hematite phase is not stable above about 625 °C. Comparison of the

$TiO_2$–$Fe_2O_3$, and $TiO_2$–FeO join (Lindsley, 1976) suggests a composition close to hematite for this phase, as in the former system hematite is stable below 585 °C and in the latter, ilmenite is stable below about 1140 °C. This is in general agreement with the composition obtained from the cell dimensions.

The fact that G.P. zones form at temperatures very close to the solvus temperature for the hematite (i.e. the depression of the solvus for G.P. zones is small) indicates that the degree of supersaturation required for their formation is not significantly greater than for the formation of hematite. This further implies that there must be a sharp free-energy minimum associated with the $TiO_2$ composition, and that a small concentration of iron is sufficient to supersaturate rutile with respect to the exsolution of an iron-bearing phase. The reasoning behind this conclusion is based on the relationships between *TTT* curves, phase diagrams, and free-energy–composition curves and is discussed in a number of standard physical metallurgy texts (Shewmon, 1969, p. 306; Verhoeven, 1975, p. 386).

The most important aspect of the exsolution process that relates to the paragenesis of the rutiles is illustrated by the shape of the *TTT* curve. An outline of the nucleation rate theory, which explains the *C*-curve shape of experimentally determined *TTT* curves is given in the Appendix. The method by which such a curve can be used to determine the free-energy barrier for the formation of a critical nucleus at any temperature, as well as the activation energy for diffusion is also briefly described. The first value determines the rate of exsolution at temperatures near the solvus temperature, whereas the second determines the way in which this rate changes as the temperature falls. Fig. 5 shows the plot of ln $t$ against the reciprocal of the absolute temperature $1/T$ for the G.P. zone curve shown in fig. 4. Using this plot and the method described in the Appendix, the minimum free-energy barrier for the nucleation of coherent precipitates (corresponding to the nose of the curve) is found to be $1{\cdot}0 \times 10^4$ J. mole$^{-1}$ °C$^{-1}$. The activation energy for diffusion, which controls the nucleation rate at temperatures below the nose of the *TTT* curve is found to be $22{\cdot}8 \times 10^4$ J. mole$^{-1}$ °C$^{-1}$. The immediate consequences of the low value for the energy barrier to nucleation and the high value for the activation energy are that at temperatures approaching the solvus the exsolution process will be rapid, but as the temperature decreases there will be a rather sharp kinetic cut-off. The slope of the *TTT* curve indicates that at temperatures below about 450 °C no significant exsolution will occur, even over very long periods. Assuming that the activation energy for diffusion is the same for the three precipitate phases, i.e. that the diffusion mechanism is the same, the kinetic cut-offs for the formation of the intermediate phase and the hematite phase will be correspondingly higher, as can be seen from fig. 4. An approximate estimate for the cut-off temperature for hematite exsolution is around 525 °C.

A note of caution is necessary with regard to the application of the present results to the general case of hematite exsolution from rutile. This concerns the factors that may affect the kinetics of the process. In the *in situ* experiments on very thin flakes in the electron microscope, nucleation of the coherent precipitates was very rapid and very dense in comparison to the annealing experiments on bulk samples. This is most likely due to the relatively large surface area to volume ratio, thus providing a far greater number of nucleation sites at the surface of the grain. Furthermore, diffusion rates are also known to be more rapid in thin films due to the lower activation energy for diffusion in the surface (Buravikhin *et al.*, 1977). The activation energy for diffusion depends on the mechanism of diffusion, and while it is considered that in the longer term annealing experiments carried out here (on grains of P32 of average grain size 0·1 mm) the dominant mechanism was volume diffusion, a decrease in grain size may well result in grain-boundary diffusion being the dominant process especially at lower temperatures. This would significantly alter the kinetics, as the activation energy for grain-boundary migration is normally much lower than that for migration through the structure. A number of annealing runs on crushed grains confirmed that the kinetics of the exsolution were more rapid, but this dependence was not rigorously examined.

A second point concerns the effect of trace elements such as the vanadium on the kinetics of exsolution of hematite. Although it is not considered likely that the presence of vanadium plays any direct role in the exsolution process observed here, its presence may alter the vacancy concentration in the rutile, hence providing more sites for the homogeneous nucleation of the precipitates. Such effects have been studied in metals (Martin and Doherty, 1976, p. 49), where it is recognized that in some systems as little as 0·1 atom% of a trace element may affect the kinetics and the nature of the precipitates.

Finally, the experiments were carried out in the absence of a vapour phase, whereas in a natural hydrothermal system, a vapour phase may have affected the kinetics of diffusion processes.

*Paragenesis of the rutiles.* The rutiles examined in the experimental part of this study were mostly of

the polygonal type. It was not possible to separate the included types because of their exceedingly fine-grained nature. Thus the group studied all belong to the phase of deposition that represents the major period of formation of the hydrothermal system. P23 is the exception, being from a partly altered granitic rock.

Preliminary studies of primary fluid inclusions indicate temperatures of deposition for the quartz in the system from about 350 to 420 °C, and by implication and textural interpretation the rutiles must have formed at similar temperatures. Secondary fluid inclusions indicate a later event, which occurred at temperatures of 300–20 °C. Although the rutiles display a range of textural settings in the rocks, the upper and lower ranges of deposition probably do not exceed the ranges indicated by the fluid inclusion studies and thus the bulk of the deposition has occurred over a limited temperature range.

The independent fluid-inclusion studies and the textural relationships confirm the temperatures of formation indicated by the annealing experiments on the exsolution process. These experiments clearly imply that, apart from P23 in which exsolution had already begun, none of the rutile specimens examined had formed at a temperature above about 450 °C. The presence of coherent lamellae in P23 implies a temperature of formation above 450 °C but below about 500 °C at which the intermediate phase would have formed. Thus P23, which appears to have a texture consistent with an interpretation of a magmatic origin, is also interpreted as a hydrothermal rutile with a temperature of formation somewhat higher than the rutiles in the surrounding rocks.

Taking into account the limitations mentioned in the previous section, the presence or absence of a precipitate phase in an iron-bearing rutile can be used as an indicator of approximate temperatures of formation. In cases where the amount of precipitate phase may be very small, and therefore the precipitates difficult to locate in crushed-grain samples, a simple criterion that indicates whether precipitation has taken place is whether *in situ* annealing in the electron microscope produces coherent platelets as shown in fig. 3. When the hematite has already exsolved, no such further precipitation occurs. This was found to be a reliable indicator of hematite exsolution in the experimental runs, even before the hematite precipitates themselves were located.

The results described in this paper indicate that a very small amount of Fe in solid solution in rutile at low temperatures is sufficient to supersaturate it with respect to exsolution of an iron-bearing phase. As most rutile analyses show the presence of some Fe, this conclusion coupled with the kinetics of the exsolution process has important implications in the paragenesis of rutiles and the conditions under which Fe may be taken up into solid solution. Preliminary investigations of some rutiles from Graves Mountain, Georgia, which have a similar origin to the rutiles described here, confirm that those rutiles observed have also formed below about 450 °C. Studies on rutiles from a variety of environments are in progress.

*Appendix*

*A TTT plot* describes the progress of a transformation on a graph of temperature ($T$) against time ($t$). A logarithmic time axis is generally used because of the wide variation in times which may be involved. The shape of a $TTT$ curve for a thermally activated process such as nucleation is governed by Becker's equation for the nucleation rate (see Christian, 1975, p. 438):

$$I = C\exp(-\varepsilon/kT)\exp(-G_c/kT) \qquad (1)$$

where $I$ = nucleation rate, $C$ = constant, specific to a given system, $\varepsilon$ = activation energy for diffusion, $k$ = Boltzmann's constant, $T$ = temperature, $G_c$ = free energy barrier for the formation of a critical nucleus.

The temperature dependence of $I$ arises through two factors: The term $\exp(-\varepsilon/kT)$ decreases rapidly with decreasing $T$, since $\varepsilon$ is a constant; and the value of $G_c$ is inversely proportional to the square of the undercooling $\Delta T$, i.e. as the temperature decreases $G_c$ decreases. Thus at the critical temperature $\exp(-G_c/kT)$ is zero and it increases continuously as $T$ decreases. The combined effect is that at the critical temperature the nucleation rate is zero; as $T$ decreases it passes through a maximum where the quantity $(\varepsilon+G_c)/kT$ is minimized, and decreases continuously as the temperature further decreases. This results in the typical C-curve of $TTT$ diagrams in which the nucleation rate at temperatures above the 'nose' of the curve is dominated by the free-energy barrier to nucleation, while at temperatures below the nose the rate is dominated by the activation energy for diffusion.

$$\text{From eqn. (1), } \ln I = \ln C - (\varepsilon/kT) - (G_c/kT) \qquad (2)$$

On the assumption that the time $t$ for a given fraction to transform is inversely proportional to the nucleation rate, we may write

$$\ln t = (\varepsilon/kT) + (G_c/kT) - \ln C^1 \qquad (3)$$

$$\frac{d(\ln t)}{d(1/T)} = \frac{\varepsilon}{k} + \frac{G_c}{k} + \frac{1}{kT}\left[\frac{d(G_c)}{d(1/T)}\right]$$

For low $T$, $G_c \approx 0$, and

$$k\left[\frac{d(\ln t)}{d(1/T)}\right] = \varepsilon. \qquad (4)$$

Thus a plot of $\ln t$ against $1/T$ enables the activation energy for diffusion to be found from the slope of the

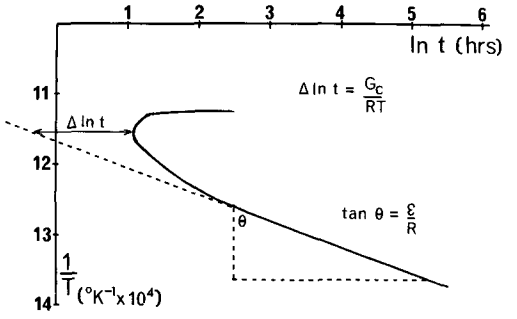


FIG. 5. Plot of ln $t$ against the reciprocal of the absolute temperature $1/T$ for the G.P. zone curve in fig. 4.

linear part of the curve at lower $T$. This is shown in fig. 5. The values obtained in the text are in molar quantities, as k has been replaced by the gas constant $R$.

The linear part of the curve has the equation:

$$\ln t = \varepsilon/kT - \ln C^1. \quad (5)$$

From 3 and 5, $G_c = kT\,[\Delta \ln t]$.

This enables the free-energy barrier for nucleation to be determined at any temperature $T$, as shown in fig. 5.

*Acknowledgements.* M. M. W. would like to thank the Department of Mineralogy and Petrology, Cambridge for facilities made available to him, and A. P. acknowledges the award of a Fellowship from the Natural Environment Research Council. We would like to thank Dr. J. D. C. McConnell for critically reading the manuscript.

## REFERENCES

Buravikhin (V. A.), Litvintsev (V. V.), and Ushakov (A. I.), 1977. Polymorphic transformations and physical properties of thin films. *Phys. stat. sol.* (*a*), **40**, 11–27.

Chadwick (G. A.), 1972. *Metallography of phase transformations.* Butterworths.

Champness (P. E.) and Lorimer (G. W.), 1976. Exsolution in silicates, 174–204. *In* Wenk (H. R.), ed. *Electron microscopy in mineralogy*, Springer-Verlag, Berlin.

Christian (J. W.), 1975. *The theory of transformations in metals and alloys*, 2nd edn. Pergamon Press, Oxford.

Connah (T. H.), 1957. Lode rutile, Mount Perry. *Queensland Govt Min. J.* **58**, 909–11.

Deer (W. A.), Howie (R. A.), and Zussman (J.), 1966. *An introduction to the rock-forming minerals.* Longman.

Denaro (T.), 1976. The geology of the Mount Perry rutile deposits. Department of Geology, University of Queensland. Unpublished Honours Thesis.

El Goresy (A.) and Ramdohr (P.), 1975. Subsolidus reduction of lunar opaque oxides: Textures, assemblages, geochemistry and evidence for a late-stage endogenic gaseous mixture. *Proc. 6th Lunar Sci. Conf.* **1**, 729–45.

Esphenshade (G. H.) and Potter (D. B.), 1960. Kyanite, sillimanite and andalusite deposits of the southeastern States. *U.S. Geol. Surv. Prof. Pap.* **336.**

Geijer (P.), 1963. Genetic relationships of the paragenesis $Al_2SiO_5$-lazulite-rutile. *Ark. Miner. geol.* **3(24)**, 423–64.

Gross (E. B.) and Parwell (A.), 1968. Rutile mineralization at the White Mountain andalusite deposits, California. Ibid. **4(29)**, 493–7.

Haggerty (S. E.), 1976. Opaque mineral oxides in terrestrial igneous rocks, pp. Hg 101–277 in Rumble (D.), ed. *Oxide Minerals*, Min. Soc. Am. Short Course Notes, **3.**

Kandiah (K.), Smith (A. J.), and White (G.), 1975. A pulse processor for X-ray spectrometry with Si(Li) detectors. Paper 2.9 *2nd ISPRA Nuclear Electronics Symposium*, Stresa, Italy.

Lindsley (D. H.), 1965. Iron-titanium oxides. *Carnegie Inst. Washington Year Book*, **64**, 144–8.

—— 1976. The crystal chemistry and structure of oxide minerals as exemplified by the Fe-Ti oxides, pp. L 61–88 in Rumble (D.), ed. *Oxide Minerals*, Min. Soc. Am. Short Course Notes, **3.**

Martin (J. W.) and Doherty (R. D.), 1976. *Stability of microstructure in metallic systems.* Cambridge University Press.

Putnis (A.), 1977. The mechanism of exsolution of hematite from natural iron-bearing rutiles. Submitted to *Phys. Chem. Minerals.*

Ross (C. S.), 1941. Occurrence and origin of the titanium deposits of Nelson and Amhurst Counties, Virginia. *U.S. Geol. Surv. Prof. Pap.* **198.**

Shewmon (P. G.), 1969. *Transformations in metals.* McGraw-Hill.

Statham (P. J.), 1976. A comparative study of techniques for quantitative analysis of the X-ray spectra obtained with a Si(Li) detector. *X-ray Spectrometry*, **5**, 16–28.

Verhoeven (J. D.), 1975. *Fundamentals of physical metallurgy.* Wiley.

Wittke (J. P.), 1967. Solubility of iron in rutile. *J. Am. Ceram. Soc.* **50**, 586–8.

[*Manuscript received 7 December 1977; revised 14 February 1978*]